ON THE ROBOTIC UNCERTAINTY OF FULLY AUTONOMOUS TRAFFIC

Hangyu Li
Intelligent Transportation Thrust, System Hub
The Hong Kong University of Science and Technology (Guangzhou)
Nansha, Guangzhou, 511400, Guangdong, China
The Hong Kong University of Science and Technology
Hong Kong SAR, China
hangyu.li@connect.ust.hk

Xiaotong Sun, Ph.D., Corresponding Author
Intelligent Transportation Thrust, System Hub
The Hong Kong University of Science and Technology (Guangzhou)
Nansha, Guangzhou, 511400, Guangdong, China
Department of Civil and Environmental Engineering
The Hong Kong University of Science and Technology
Hong Kong SAR, China
xtsun@ust.hk

Word Count: 6504 words + 1 table(s) $\times$ 250 = 6754 words

Submission Date: July 3, 2022

ABSTRACT

Macroscopic traffic flow analysis usually assumes that autonomous vehicles (AVs) preserve perfect microscopic behaviors. This allows AVs to maintain shorter headways than human-driven vehicles, resulting in a greater capacity for the overall traffic if the market penetration is sufficiently high. Nevertheless, as a special class of ground robots, autonomous vehicles are inevitably subject to errors in their operation, particularly in perception, causing inconvenient uncertainty in their movements. With this deficiency, current automated vehicles on the road often sacrifice efficiency for safety by employing conservative operations strategies. Such strategies include long car-following distances, frequent emergency braking actions and cautious lane changing strategies, which nullify the desired systematic benefits of fully- or mixed- autonomous traffic.

To reconcile the inconsistency above, we propose an analytical model framework that describes the endogenous relationship between safety and capacity that arises from robotic uncertainty in AVs. Our study focuses on the fully autonomous environment, where the propagation of uncertainty from an AV's perception to its movement is first established. The collision rate due to uncertain movements is then derived, providing an explicit link between safety and traffic capacity. Finally, the relationship between safety and capacity is streamlined over traffic density, one of the most fundamental metrics of traffic flows. Specifically, we substantiate the model framework in the car-following scenario, where only forward perception, longitudinal movements, and the rear-end collision are considered. Correspondingly, the mathematical dependence of traffic capacity and safety are described as a function of headway under different designated speed. This model further enables us to balance the trade-off between safety and traffic capacity for traffic management purposes. The choice of either conservative or aggressive operational policies determines whether we optimize safety performance that meets capacity requirements or maximize traffic capacity within an acceptable range of collision rate. In reverse, given the expected performance of traffic safety and efficiency, this model also indicates the maximum tolerable uncertainty of AVs, contributing to the testing and development of the technology.

Keywords: autonomous vehicles, robotic uncertainty, traffic capacity, collision rate, sensor error

INTRODUCTION

The advent of autonomous vehicles (AVs), or fully automated vehicles, offers the potential to improve both the overall traffic safety and efficiency (*1, 2*). AVs with intelligent decision-making abilities and accurate machinery operations will be able to prevent accidents caused by human errors, which is identified as the main cause of car crashes (*3*). When investigating their impact on traffic efficiency, AVs are usually treated as ideal machines with more advanced driving capabilities. Accordingly, AVs are assumed to maintain a shorter stable headway in traffic streams than human-driven vehicles (HDVs) (*4*), contributing to different levels of increased roadway capacity relevant to their market penetration (*5–9*).

However, AVs are prone to systematic errors due to their robotic nature. Like other ground robots, AV operations typically consist of four modules: perception, localization, planning (or decision-making) and control (*10–12*). Each of these modules introduces a certain degree of uncertainty, resulting in a deviation between an AV's real position and its designed one. The potential harm on traffic safety caused by this deficiency has prompted research on more intelligent modules that can improve AVs' operational accuracy. For instance, Thrun (*13*) used Bayes' theorem to estimate the state of the vehicle, and derived the most likely position for decision-making reference. Kalman Filter was adopted to reduce the overall error by fusing multiple sensor data together Roumeliotis and Bekey (*14*). The uncertainty has also been considered in adaptive cruise control (ACC) and cooperative adaptive cruise control (CACC) to form a better platoon performance (*15*). A more comprehensive review could be found in (*16–18*).

Meanwhile, autonomous driving companies are taking a much more conservative approach when testing their pilot vehicles in practice. The lack of clear laws and regulations on AV operations (*19*), coupled with public concerns on autonomous driving accidents (*20–22*), prevent profit-driven companies from deploying more advanced technologies in the field tests. Compared with HDVs, these pilot vehicles are driving slower, and keeping longer car-following distances on road, sacrificing the traffic efficiency in exchange for safety.

In light of all these facts, this paper aims to investigate the mutual relationships between traffic efficiency and safety performance in a fully autonomous-vehicle environment, with robotic uncertainties as a determining factor. We first build a conceptual model framework, starting with the stochastic propagation formulation of errors originating from perception, the module thought to have the greatest impact on AV movement accuracy (*23, 24*). In this way, we can establish a relationship between traffic density and collision rate, connecting traffic capacity and safety at a macro level. A car-following scenario further substantiates the conceptual model, in which only forward perceptions, longitudinal movements, and rear-end collisions are considered. As a result, the average capacity and collision rate can be explicitly formulated by two simple parameters, bump-to-bump distance, and the associated average speed.

Considering the stochastic nature of traffic flows is not a new thing in literature. To name a few, Krauß (*25*) considered the variance capabilities of acceleration and deceleration in modeling a stochastic microscopic car-following model; Jabari and Liu (*26*) proposed a macroscopic traffic flow model with state-dependent time headways; Xu and Laval (*27*) modeled the acceleration error process as a Brownian motion. However, most of them consider randomness to be attributed to the heterogeneity of human drivers, and some resort to non-stationary traffic states observed in aggregated traffic data (*28*). In contrast, AVs have no such heterogeneous intentions. And to the best of the authors' knowledge, the essential systematic robotic errors of AVs have not been covered, and this paper serves as the first attempt to incorporate AVs' robotic uncertainty in the traffic flow analysis.

Unlike most accident-free traffic models proposed previously, this paper explicitly uses accident-inclusive traffic capacities to represent traffic efficiency, with AVs' robotic errors as the only sources of accidents. In addition, since we are interested in the maximum capacity that can be offered by AV technology, we do not consider the effect of demand on the realized traffic efficiency. The derived analytical model are expected to quantify the magnitude of robotic errors on the integrated traffic efficiency and safety performance, which is promising to bring insights on the accuracy of autonomous driving sensors and algorithms.

The structure of this paper is organized as follows. We first establish a general conceptual model from error propagation to the formation of the relationship between traffic capacity and safety. Then a car-following specification of this model is given, followed by mathematical analyses and discussions. We draw our conclusions in the end.

THE GENERAL MODEL FRAMEWORK

In this section, we first present the conceptual framework of the stochastic propagation through the four modules of AV operations. Based on that, the safety performance and the efficiency performance of an autonomous traffic are derived.

Stochastic movements of AVs

Error propagation

Before planning its local route and movement, an autonomous vehicle perceive the surrounding environment to localize itself. In equation (1a), we denote the set of the actual position and the geometric relationship of object around as $\mathbf{P}$. When employing multiple sensors like cameras, radars, Lidars to observe objects around, there exists a certain degree of error in the observation , shown as ε_O^i, $\forall i$ in (1b), due to sensors' accuracy limitation. In (2a) - (2b), L represents the localization function used by the ego autonomous vehicle and an estimation p_{ego}^e could be made with the set of observation $\mathbf{P}^o$. Therefore, a deviation between the estimated position and the actual position would exist, expressed by ε_L in (2c).

$$\mathbf{P} = \{p_i | i = 1,2,3,...\} \tag{1a}$$

$$\mathbf{P}^o = \{p_i^o | p_i^o = p_i + \varepsilon_O^i, i = 1,2,3,...\} \tag{1b}$$

$$p_{ego} = L(\mathbf{P}) \tag{2a}$$

$$p_{ego}^e = L(\mathbf{P}^o) \tag{2b}$$

$$p_{ego}^e = p_{ego} + \varepsilon_L \tag{2c}$$

In (3a) and (3b), the decision function D implies that the decisions of autonomous vehicles, acceleration, steering, etc., are made according to the position of surrounding objects and its own location. Decision-making function is shown as In addition to the localization error, the decision of autonomous vehicles based on perception and localization would also have some offset, resulting in a deviation, of ε_D between the actual motion of the autonomous vehicle and the designed one denoted in (3c).

$$u_{ego} = D(\mathbf{P}, p_{ego}) \tag{3a}$$
$$u^e_{ego} = D(\mathbf{P}^o, p^e_{ego}) \tag{3b}$$
$$u^e_{ego} = u_{ego} + \varepsilon_D \tag{3c}$$

Stochastic motion

Thus, given the same conditions, the stochastic motion will cause the ego AV to appear in various possible positions in the space. Note that, although we write the stochastic motion of autonomous vehicle as shown in (3c), this does not mean that a series of random motions are simply additive, as it will lead to infinite error growth and systematic instability. Indeed, it is an issue that needs careful treatments in the control module, which is beyond the scope of this paper. We instead assume a stable AV operation system, where the uncertainty of position converges to a fixed time-invariant distribution, as shown in (4).

$$p_{ego} = p^* + \varepsilon_P \sim \mathscr{X} \tag{4}$$

In practice, the distribution $\mathscr{X}$ is jointly determined by sensing accuracy and autonomous driving algorithms, reflecting the ability of an AV. Under the same level of sensing accuracy, the more advanced the driving algorithm is, the smaller the variance of ε_P, indicate that the actual position distribution of a AV p_{ego} is more concentrated around the designed position p^*. In this paper, we assume that the optimal driving algorithm is adopted, so that p_{ego} is mostly determined by sensing accuracy.

Measurement of traffic safety

We use the probability of collision, which equals to the collision rate in macro statistics, to uniformly quantify the AV safety performance. As shown in (5), two factors contribute to the probability of collision, P_c. One is the distribution of possible positions, $\mathscr{X}$, determined by the precision of sensors. Another is the collision region, C, indicating the dangerous region where collision could happen. The integral variable p indicates the possible positions that the ego AV could appear, and $f_{\mathscr{X}}$ is the probability density function of distribution $\mathscr{X}$.

$$P_c = \int_{p \in \mathbf{C}} f_{\mathscr{X}}(p)\mathbf{d}p \tag{5}$$

Notice that both P_c and C are affected by the complex geometric relationship of angles and distances between rigid vehicle bodies, $\mathbf{P} \bigcup p_{ego}$, which can be statistically approximated by with the variance term $\sigma_{\mathscr{X}}$ and the overall traffic density k in the region, leading to a simplified formed of collision rate in (6).

$$P_c = F^{\mathbf{C}}_{\mathscr{X}}(k) \tag{6}$$

Here, we assume that $\frac{dF^{\mathbf{C}}_{\mathscr{X}}(k)}{dk} > 0$, as a higher value of traffic density means closer vehicle-to-vehicle distances, leading to a higher collision probability. We further assume that $\lim_{k \to \infty} F^{\mathbf{C}}_{\mathscr{X}}(k) = 1$ and $\lim_{k \to 0} F^{\mathbf{C}}_{\mathscr{X}}(k) = 0$, implying that the extremely high density would almostly lead to collisions, if the speed has been unchanged, and the extremely low density would eliminate the possibility of all collisions [1].

The accident-inclusive traffic capacity

As shown in (7), a roadway capacity is the maximum attainable traffic flow rate under the equilibrium condition, which is the product of density k and speed v. In conventional human-driven traffic streams, the equilibrium speed v is endogenously determined by density k, since drivers would slow down to avoid collision in high density scenarios, leading to a back-bending curve between flow rate and density in the fundamental diagram (*29*).

$$s^+ = \max kv(k) \tag{7}$$

Comparatively, the capacity of fully autonomous traffic differ from that of human-driven traffic in two ways. First, high density scenarios in human-driven traffic stem from high traffic demand. In fully autonomous traffic, as the demand consideration is excluded, the traffic density is directly determined by vehicle-to-vehicle distance, minimum time gap, which are parameters set by autonomous driving algorithms. Second, AVs could maintain high speeds even at a relatively high density traffic due to the more advanced driving capabilities. As a result, speed v and density k in (7) can be decoupled. With that, we now adjust the capacity formulation as that in (9a), where k^a and v^a indicate the maximum density and speed allowed by the autonomous driving algorithm.

$$s^+ = k^a v^a \tag{8}$$

Treating the robotic error as the only source of collisions, we then derive the reduced accident-inclusive capacity for fully autonomous traffic as follows.

$$\bar{s} = \bar{\eta} s^+ \tag{9a}$$

$$\bar{n} = T\bar{s} \tag{9b}$$

$$\begin{aligned} \mathbb{E}s &= s^+ - \frac{1}{\tau}\bar{n}P_c\mathbb{E}s \\ &= \frac{k^a v^a}{(1+\bar{\eta}TF(\sigma_{\mathscr{X}},k)k^a v^a/\tau)} \end{aligned} \tag{9c}$$

In (9a), the reduced capacity $\bar{s}$ is given by the reduced proportion of full capacity, $\bar{\eta}$. The reduced proportion is influenced by many factors, such as the number of lanes on the roadway. Accordingly, reduced flow (number of passing vehicles), $\bar{n}$ could be obtained in (9b) by using reduced capacity times total influenced time, which is assumed to be equal to the total clearance time T of the accident. Modeling the AV operation as a discrete system with time step τ, the total number of collisions could be calculated as total number of vehicles times their collision rate at each study period divided by the processing time step. In the equilibrium state, the relationship in (9c) holds, and analytical expression of expected average capacity $\mathbb{E}s$ can be derived.

CAR-FOLLOWING SPECIFICATIONS

So far, we have established all the mathematical formulations of the conceptual model, providing a general method to analyze accident-inclusive capacity with AV uncertainty, regardless of the traffic scenarios. However, as it is impossible to use a uniform micro mathematical model to represent

[1] Though the specific format of $F_{\mathscr{X}}^{\mathbf{C}}(k)$ is determined by the traffic conditions and the error distribution function being specified, a sigmoid- or erfc-like function with respect to traffic density can be a good fit to the inherent properties of error distributions.

AVs' movement in all traffic scenarios, we specifically study the car-following scenario in the following sections. The propagation of internal robotic error and its impact on collision rates will be established in a clearer way.

Scenario establishment

We first establish the car-following scenario under the following assumptions:

1. *Forward perception.* Only the influence of the front vehicle is taken into account for the ego vehicle. Perceptual information other than measurements of the front vehicle is ignored. In addition, we do not specify the internal processing of the sensors, but only keep the perceptual information that can be used by downstream algorithms.
2. *Longitudinal control.* Control of AVs can be divided into longitudinal and lateral ones. The former one is responsible for the acceleration and braking of the vehicle, while the latter one controls the steering angle. Our study focuses only on the longitudinal car- following and the influence of left and right traffic is excluded. In the meantime, the correlation between lateral and longitudinal control on curves caused by vehicle dynamics is also not examined.
3. *Rear-end collision.* With the previous two assumptions, the reduction on traffic capacity is purely attributed to the rear-end collisions that occur in a single lane, and no vehicles in adjacent lanes will be involved in the accident. Therefore, the lane where accidents happened will be directly blocked, reducing its capacity to zero, and capacities on other lanes are deteriorated by the subsequent bottleneck phenomenon.

Automated car-following

The Car-following model

Among all the versatile car-following models developed in years, we adopt the simplified Newell's model (*30*) to mimic the car-following process of the ego autonomous vehicle. Newell model only requires the continuous observation of the front vehicle's position, according to which the position of ego vehicle can be directly adjusted. Controls on higher-order parameters, including speed, acceleration, and jerk, are realized automatically. Though unrealistic from microscopic perspective, Newell model describes the macroscopic traffic flows appropriately. As most of the analyses in this section concentrate on the equilibrium state, using Newell's model to link the traffic safety and efficiency is well accepted.

Error propagation

Assume the front vehicle starts from position x_0 and drives at a constant speed v, its trajectory dynamic could be represented as follows:

$$v_f(t) = v \tag{10a}$$

$$x_f(t) = x_0 + vt \tag{10b}$$

Equations (11)-(12), $x_f^o(t)$ represents Newell's model with observation errors. At each time t, the ego vehicle makes an observation on the position of the vehicle in front. The observation is considered to have a Gaussian error with zero mean and a variance of σ_x^2. ε_x. The movement of ego vehicle $x_e(t)$ follow the front vehicle with a delay of τ and a kept safe spacing δ. σ_x^2 and τ represent the ability of ego AV. The former represents the precision of perception, and the latter represents the perception processing and control response time. Consequently, the ego vehicle following the observed trajectory introduces randomness into its own movement.

$$x_f^o(t) = x_0 + vt + \varepsilon_x \tag{11}$$
$$\varepsilon_x \sim \mathcal{N}(0, \sigma_x^2)$$

$$\begin{aligned} x_e(t) &= x_f^o(t-\tau) - \delta \\ &= x_0 + vt - v\tau + \varepsilon_x - \delta \end{aligned} \tag{12}$$

Expression of distance

Combining (11)-(12), we can derive the actual distance of two vehicles at time t.

$$\begin{aligned} d(t) &= x_f(t) - x_e(t) \\ &= \delta + v\tau - \varepsilon_x \end{aligned} \tag{13}$$

Considering that the safety distance varies with speed, the safety time headway is a more general variable to render the degree of driving aggressiveness. Moreover, time headway is monotonically decreasing with respected to a single-lane capacity. For theses reasons, we reformulated the safe distance in (13) to a function of safe time headway in (14). It should also be noted that the distance between two vehicles is independent of time, which means, from a macro point of view, the observation of the distance between two vehicles at any time follows the same stochastic manner. Therefore, we can rebuild it as a time invariant function of h^a and v^a in (15).

$$d(t) = vh + v\tau - \varepsilon_x \tag{14}$$

$$\begin{aligned} d(v,h) = d(t) &= (h+\tau)v - \varepsilon_x \\ &\sim \mathscr{D} = \mathcal{N}((h+\tau)v, \sigma_x^2) \end{aligned} \tag{15}$$

So far, we have given the random motion of the ego vehicle, as shown in Figure 1. The Gaussian distribution from the observation error preserves, with a mean time the headway being $h+\tau$ and a mean spacing being $(h+\tau)v$.

Measurement of traffic safety

In the homogeneous autonomous traffic where all vehicle length are the same, real-end collisions occur when the head-to-head spacing $d(v,h)$ becomes less than the vehicle length. Adopting the Gaussian distribution function, equation (16) indicates the probability of collision, giving speed v and, time headway h, and vehicle length L. Since h and v only contribute to the mean of distance, equation (16) can be further simplified as a uni-variate function, denoted by (17) and (18). In the probability function, contribute only to the mean of distance, so that we can write the function

A concrete relationship is shown in the Figure 2

$$\begin{aligned} P_c(v,h) &= F_{\mathscr{D}}^{d \le L}(v,h) \\ &= \int_{-\inf}^{L} f_{\mathscr{D}}(v,h)\mathbf{d}d \\ &= \int_{-\inf}^{L} \frac{1}{\sqrt{2\pi}\sigma_x} exp(-\frac{(d-(h+\tau)v)^2}{2\sigma_x^2})\mathbf{d}d \end{aligned} \tag{16}$$

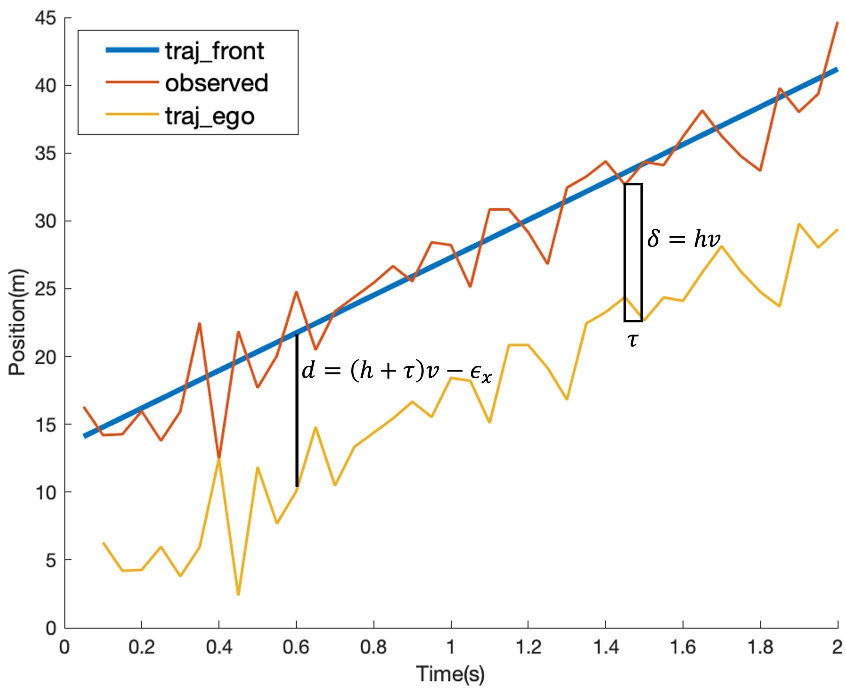

FIGURE 1 This figure shows the car following behavior according to the Newell model with perceptual error. Processing time, safe headway and spacing, and actual distance are shown in the figure.

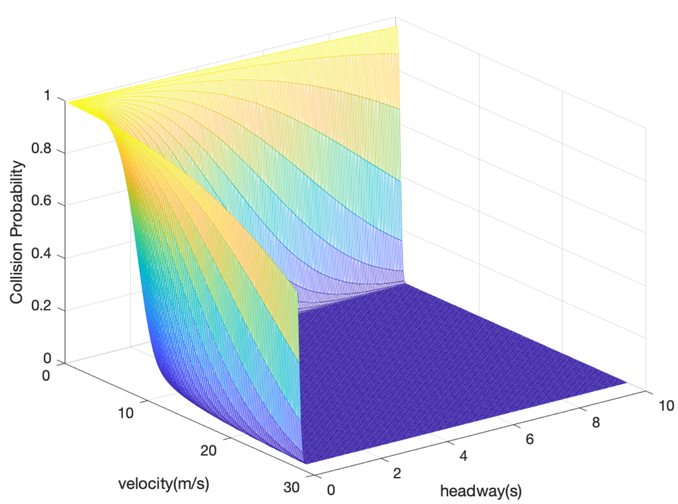

FIGURE 2 This figure shows the probability of collision with speed and safe headway.

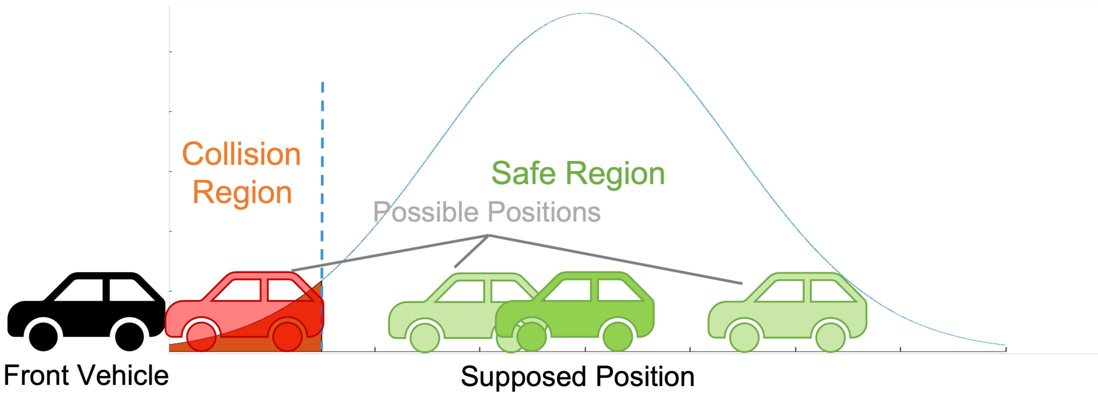

FIGURE 3 This figure shows the stochasticity of the position when following a car with a normal distribution. When the distance is less than the length of a vehicle, a rear-end collision occurs.

$$d_m = (h+\tau) \tag{17}$$

$$\begin{aligned} P_c(d_m) = P_c(v,h) &= \int_{-\inf}^{L} \frac{1}{\sqrt{2\pi}\sigma_x} exp(-\frac{(d-d_m)^2}{2\sigma_x^2})\mathbf{d}d \\ &= \int_{-\inf}^{L-d_m} \frac{1}{\sqrt{2\pi}\sigma_x} exp(-\frac{d^2}{2\sigma_x^2})\mathbf{d} \end{aligned} \tag{18}$$

With a fixed mean of distance d_m, the probability of collision would remain unchanged. It means that to maintain the safety performance, increasing speed forces the shortening on time-headway, and vice-versa. However, it does not mean that the *severity* of collision would be the same, as the momentum in collision increases with respect to the traveling speed.

$$\frac{\partial P_c(v,h)}{\partial v} = \frac{\mathbf{d}P_c(d_m)}{\mathbf{d}d_m}\frac{\partial d_m}{\partial v} = -\frac{h+\tau}{\sqrt{2\pi}\sigma_x} exp(-\frac{((h+\tau)v-L)^2}{2\sigma_x^2}) \tag{19a}$$

$$\frac{\partial P_c(v,h)}{\partial h} = \frac{\mathbf{d}P_c(d_m)}{\mathbf{d}d_m}\frac{\partial d_m}{\partial h} = -\frac{v}{\sqrt{2\pi}\sigma_x} exp(-\frac{((h+\tau)v-L)^2}{2\sigma_x^2}) \tag{19b}$$

Equations (19a) and (19b) further quantify the negative marginal contributions of v and h to the collision probability, respectively. Meanwhile, at high speed, the change rate of collision probability with h is greater in critical cases, indicating greater difficulty in control of h, which will be analyzed in more details in the discussion section.

The accident-inclusive capacity

Following the practice in the general model, we provide the capacity with rear-end collisions as follows

Full capacity

Ideally, as mean of headway being $h+\tau$, the lane capacity could be derived without the consideration of collisions.

$$s^{+}(h) = \frac{3600}{h+\tau} \tag{20}$$

Reduced capacity
Once a traffic accident occurs, a lane would be temporarily blocked, resulting in a bottleneck and reduced traffic capacity. Unfortunately, the microscopic dynamic characteristics of AVs under accidents could be complicated, which is also fall short of data. As a remedy, we adopt use the historical data of human driven traffic accidents shown in Table 1 from North Virginia (*31*) to quantify the impact of lane blocking on traffic capacity.

TABLE 1 Remaining proportion of capacity when lane blocking

Number of Lanes	One Lane Blocked	Two Lane Blocked	Three Lane Blocked
2	0.39	0.00	N/A
3	0.45	0.17	0.00
4	0.58	0.25	0.13
5	0.65	0.40	0.20
6	0.71	0.50	0.26
7	0.75	0.57	0.36
8	0.78	0.63	0.41

$$\eta_N^M = \frac{N-M}{N+M} \tag{21}$$

Equation (21) represents remaining proportion of capacity, η_N^M, when M lanes are blocked simultaneously on a road with total N lanes. For $M = 1,2,3$, the results of data fitting are shown in the Figure 4. The R-square of the three are 0.9977, 0.9691 and 0.8979 respectively.

As trying to focus on the lane that the ego AV drives on, we ignore the situation that multiple lanes are blocked at the same location at the same time. Such a treatment is acceptable since multi-lane blocking is an event with extremely small probability.

$$\eta_N = \frac{N-1}{N+1} \tag{22a}$$

$$\bar{\eta}_N = 1 - \eta_N = \frac{2}{N+1} \tag{22b}$$

$$s_N(h) = \eta_N s^{+}(h) = \frac{N-1}{N+1}\frac{3600}{h+\tau} \tag{23a}$$

$$\bar{s}_N(h) = \bar{\eta}_N s^{+}(h) = \frac{2}{N+1}\frac{3600}{h+\tau} \tag{23b}$$

The remaining proportion of capacity when a single lane blocked is shown in (22a), while the reduced proportion is shown in (22b) accordingly. With the proportion and the full capacity, remaining capacity and reduced capacity could be written as (23a) and (23b) respectively.

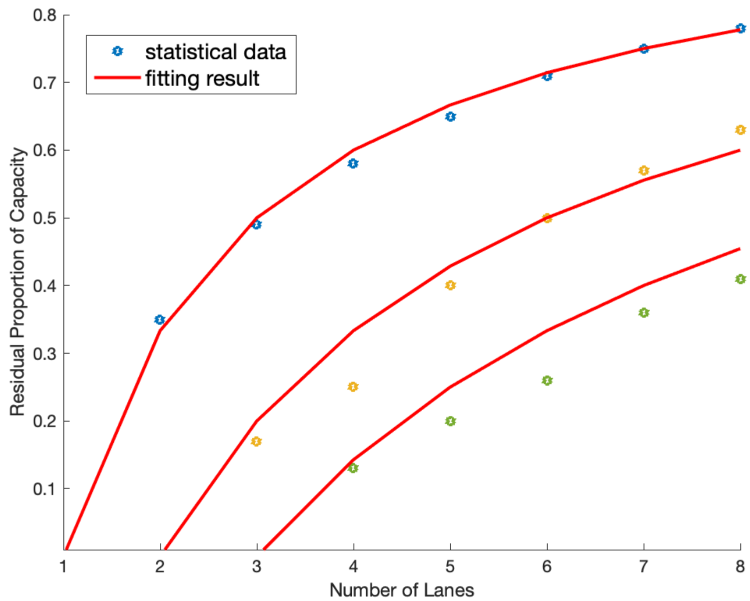

FIGURE 4 This figure shows the fitting results according to the real statistical data of a tech report from North Virginia

Collision clearance time

Noticing that the lane blocking is temporarily, we introduce the total clearance time (TCT), during which the reduced capacity takes effect. As the name suggested, the total clearance time represents the time duration from the occurrence of the accident to the complete clearance of the accident site (*32*).

At present, there are few literature to model the accident dealing process for fully autonomous vehicles. Intuitively, the TCT of AV collisions is positively related to their severity, which is positively related to the traveling speed. Since the sensors may be damaged after the collision, AV cannot resume operations in a short time, resulting in the existence of a minimum handling time. In contrast to HDVs, the identification of collision responsibility for AV accidents can be carried out offline and saved, due to the rich sensing information of AVs.

We refer to the composition and typical values of TCT in a tech report in North Virginia (*31*). Incorporated with the previously-introduced features of AV collisions, we then give a simple and intuitive model in (24) to represent AVs' TCT. The minimum processing time is set to 30 minutes and the maximum one to 60 minutes. For those in between, time increases linearly with speed. For the scenario applicable to car following under non free flow, we only consider its linear segment.

$$T(v) = min\{54v + 1800, 3600\} = 54v + 1800|_{v \leq 33.33m/s(120km/h)} \tag{24}$$

Since the clearance time is independent of other variables in the model, this reasonable time assumption will not change the essence of our model nor the correlation between variables.

Average capacity

Combining (23b) and (24), reduced number of passing vehicles caused by one collision could be calculated:

$$\bar{n}(v,h) = \frac{\bar{s}_N(h)}{3600}T(v) = \frac{2}{N+1}\frac{54v+1800}{h+\tau} \tag{25}$$

Finally, the expectation of total number of collisions in a certain time period could be calculated by P_c times actual number of vehicles passing in the period and the number of state transitions when passing, as considering the AVs as discrete systems. Note that, although we do not consider other interactions between lanes, the capacity of all lanes will decrease after a collision in any lane, and the mean value is calculated in (23b). Therefore, when we calculate the impact of collisions on the lane include ego vehicle, collisions on all lanes should be considered.

$$\mathbb{E}c(v,h) = P_c(v,h)\mathbb{E}s(v,h)\frac{h+\tau}{\tau}N \tag{26}$$

Combining (25) and (26), total reduced number of vehicles during the time period could be derived. The expectation of average passing number of vehicles could then be calculated as full capacity of the period minus the reduced vehicles.

$$\mathbb{E}s(v,h) = s^+(h) - \mathbb{E}c(v,h)\bar{n}(v,h) = s^+(h) - P_c(v,h)\mathbb{E}s(v,h)\frac{h+\tau}{\tau}N\frac{2}{N+1}\frac{54v+1800}{h+\tau} \tag{27}$$

$$\begin{aligned}\mathbb{E}s(v,h) &= \frac{\frac{3600}{h+\tau}}{1+P_c(v,h)\frac{h+\tau}{\tau}N\frac{2}{N+1}\frac{54v+1800}{h+\tau}} \\ &= \frac{3600}{h+\tau+\frac{2N(54v+1800)(h+\tau)}{(N+1)\tau}\int_{-\inf}^{L}\frac{1}{\sqrt{2\pi}\sigma_x}exp(-\frac{(d-(h+\tau)v)^2}{2\sigma_x^2})\mathbf{d}d}\end{aligned} \tag{28}$$

It can be seen from (28) that the expectation of average traffic capacity is greater than 0 while less than the full capacity $s^+(v,h)$. A more concrete relationship is shown in the Figure 5.

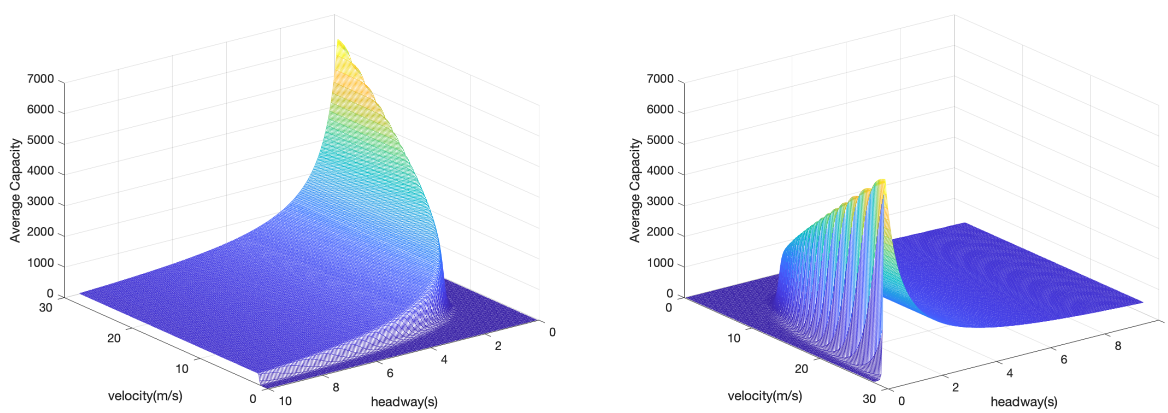

FIGURE 5 These two figures show the relationship between the expectation of average capacity and speed and safe headway in different angles

Four parameters of N, L, τ, σ_x, and two variables of v and h contribute to the final result of

$\mathbb{E}s(v,h)$. The influence of parameters on it and the optimization on variables will be analyzed and discussed in detail the subsequent sections.

The general trade-off relationship of average capacity and collision probability is shown in Figure 6.

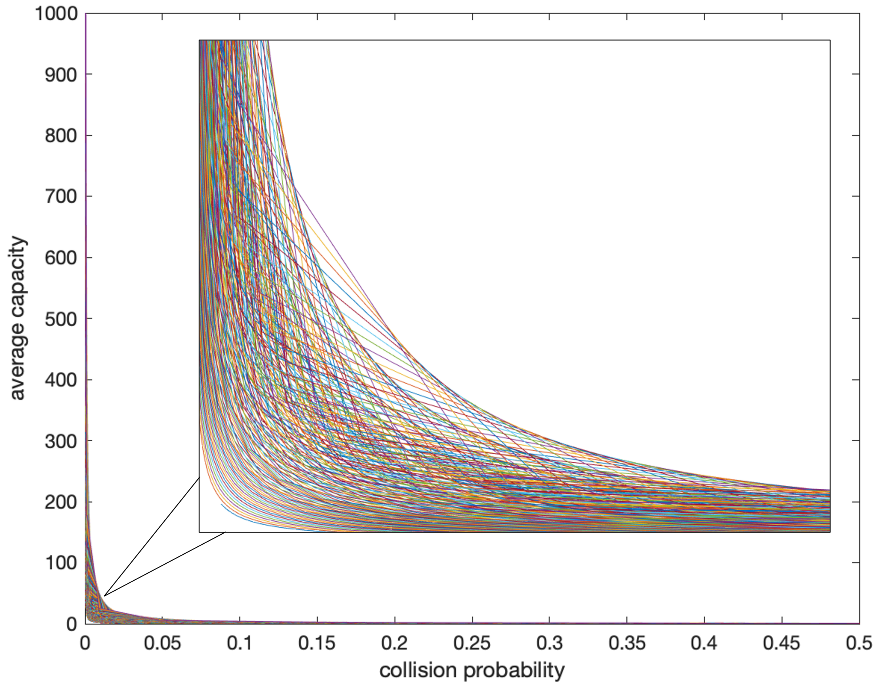

FIGURE 6 This figure shows the general trade-off relationship between traffic efficiency and safety. Each line represents a condition with certain speed or safe headway.

DISCUSSION

Influence of parameters

Among the four parameters contributed to the safety and efficiency of fully autonomous traffic shown in (16) and (28), the number of lanes N is determined by the roadway condition, while others are contributed from the vehicle perspective. Length L is an inherent property of design, while time step τ and precision σ_x represent the capability performance of autonomous vehicle hardware. In the following context, we discuss the impact of each parameter respectively.

Number of lanes (N)

In the car-following scenario, AVs' collision rate due to robotic uncertainty is irrelevant to the number of lanes on the roadway, as shown in (16). This result is aligned with our previous assumptions, where no lateral control or side impact that captures the interaction between lanes are considered.

Without doubt, the number of lanes affects the average traffic capacity $\mathbb{E}s$ by influencing the impact of accidents on traffic, with the form of $\frac{N}{N+1}$ in (27). That is, for a road with more lanes, the decrease of the average traffic capacity caused by accidents is more, while the decrease amplitude decreases with the increase of N. This is not difficult to understand as multi-lane roads need to consider the average impact of bottlenecks caused by collisions happened in other lanes. In addition, although the average lane capacity decreases with the number of lanes, the overall road capacity continues to grow. In real road design and planning, this process of diminishing marginal benefits need to be comprehensively considered with the linear growth of cost.

Length of vehicle (L)

The length of the vehicle L will have an impact on safety in (16), because we set a constant headway following model, and the headway corresponds to the head-to-head or tail-to-tail distance between vehicles. This includes the distance interval between the two and the length of the vehicle. Therefore, a longer vehicle will lead to a shorter head-to-tail distance between two vehicles, thereby increasing the probability of collision and reducing safety.

However, vehicle length L has no effect on other parts of traffic capacity in (28). Therefore, its only influence on traffic capacity is that longer vehicles lead to higher collision probability and reduce traffic capacity.

Note that, its impact on safety is not essential, but related to car-following strategies. If we consider a car following model that controls the tail-to-end distance between the front and the ego vehicle, it would have no impact on safety. However, its impact on traffic capacity remains negative, because a longer vehicle means a longer headway under the same safety conditions. Therefore, compared with vehicles with large space, compact vehicles may become more favored for full autonomous traffic in the future.

Precision of sensors (σ_x)

As the most important parameter to measure the perception ability of autonomous vehicles, the perception precision indicated by variance of perceived results σ_x is crucial to safety. With Gaussian distribution, as long as $(h+\tau)v$ is set to be greater than L, lower σ_x would lead to fewer collisions. This property remains true regardless of the driving strategy being employed. Otherwise, the strategy would be deliberately inclined to hit the front car, setting the tail-to-end distance less than 0.

Like vehicle length L, σ_x has no other impact on the average capacity. More precise sensors with less σ_x lead to safer traffic conditions and thereby allowing more efficient car-following strategies that contribute to greater traffic capacity and overall benefit.

Time step (τ)

The comprehensive time step τ includes the processing time of perceptual information, the calculation time of autonomous driving algorithms and the response time of control. Serving as the reaction time of an AV, it is also an important indicator to measure the ability of autonomous driving. The contribution of τ to the safety and capacity could be divided as two aspects.

In the first aspect, it appears together with h as a supplement to the actual macro headway. The impact on safety comes from this aspect. However, τ is too small compared with h, and has little influence on the actual headway. In most cases, its impact on safety and capacity could be negligible. In addition, such influence stays on the expression, not the essence. Defining $h_r = h+\tau$ as the actual headway would easily eliminate it, with control of headway variable remaining available.

On the other aspect, like shown in (26), τ affects the number of state changes during the passing time of the discrete AV system, which is used in calculation of collision rate. Therefore, ignoring the influence of τ on the headway, smaller τ indicates more state changes, resulting in a higher collision rate as the probability of collision in each state remains same. This shows a negative impact on capacity.

We find it inconsistent with intuition as a shorter processing time should indicate a better AV system while the advantages are not revealed. This is mostly because of the neglect of differential characteristics in the Newell car-following model. In some more detailed models, the perceptual error affects the velocity and acceleration, and the further influence of these two on the position would increase with τ. However, due to the complexity of stochastic nonlinear model, and few impact on the main content of this paper, we will continue to study it and try to cover it in another paper.

Control and optimization on variables

In the car-following scenario, we use v and h as two controllable variables. From a single vehicle perspective, its speed is restricted by the velocity of the car in front, making headway the only parameter that can be tuned. Nevertheless, once a platoon of autonomous vehicles is formed under the optimal headway h, their speed can be optimized as a whole to improve the overall traffic capacity.

Therefore, we regard the process of controlling v and h to pursue greater traffic capacity as a two-stage optimization problem.

$$\max_{v}[\max_{h}\mathbb{E}s(v,h)] \tag{29}$$

Optimal headway of the ego vehicle

At the first stage, we optimize h at a given speed v_0.

$$\max_{h}\mathbb{E}s(v_0,h) \tag{30}$$

Noticing that the numerator $\mathbb{E}s$ is a constant, we reformulate the maximization problem above as the following minimization problem (31), where the objective $S_{v_0}(h)=\frac{2600(N+1)\tau}{\mathbb{E}s(v_0,h)}$.

$$\min_{h} S_{v_0}(h) = (N+1)\tau h + [2N(54v_0+1800)(h+\tau)]\int_{-\inf}^{L-(h+\tau)v_0}\frac{1}{\sqrt{2\pi}\sigma_x}exp(-\frac{d^2}{2\sigma_x^2})\mathbf{d}d \tag{31}$$

The first order condition could be written as follows:

$$FOC:[v_0(h+\tau)\phi_{\sigma_x}(L-(h+\tau)v_0)-\Phi_{\sigma_x}(L-(h+\tau)v_0)=\frac{(N+1)\tau}{2N(54v_0+1800)} \tag{32}$$

Here, Φ_{σ_x} and ϕ_{σ_x} indicate the cumulative distribution function and the probability density function of Gaussian distribution $\mathcal{N}(0,\sigma_x^2)$, respectively. The right term of (32) is a small positive value close to 0. Considering $v_0(h+\tau)$ as d_0, there is a one-to-one correspondence between h and d_0. The left terms could be treated as a function of d_0 and decreases monotonically to the limit of 0 when $d_0 \geq L$. Therefore, one and only one $d_0^* \geq L$ exists satisfying (32). The corresponding $h^*(v_0)$ could then be derived, which serves as the optimal h that maximize the road capacity under speed of v_0.

The result of this first stage optimization could be seen in Figure 7

Note that, as v_0 grows up, the right term of (32) would be smaller, leading to a larger d_0 to

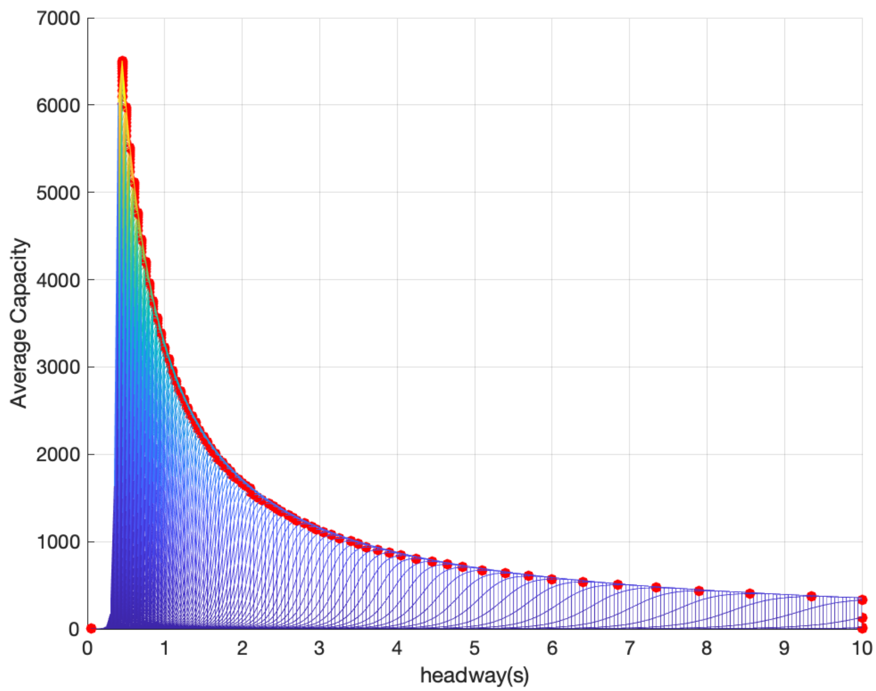

FIGURE 7 This figure shows the result of this first stage optimization. Each line shows the process of optimization made on safe headway to maximize the capacity given a certain speed. Red scatters indicate the optimal h and corresponding capacity at each speed.

satisfy it. This means that the optimal following distance at high speed is larger than that at low speed, which is consistent with intuition.

$$\frac{\mathbf{d}S_{v_0}(h)}{\mathbf{d}h} = (N+1)\tau + 2N(54v_0+1800)[\Phi_{\sigma_x}(L-(h+\tau)v_0) - v_0(h+\tau)\phi_{\sigma_x}(L-(h+\tau)v_0)] \quad (33)$$

The first-order derivative of h (33) indicates that the increase of v_0 will magnify the influence of h on the first derivative. Therefore, for h around $h^*(v_0)$ satisfying the first order condition, it will lead to a steeper change of the original function. That is, at higher speed, if the h is not controlled perfectly so as to have a deviation Δh, the proportion of capacity loss caused by this error would be greater. Therefore, this is also one of the factors representing the ability of autonomous driving, which is worthy of further research.

Optimal speed of the vehicle platoon

As we discussed before, for each speed v_0, an optimal $h^*(v_0)$ satisfying (32) could be derived to maximize the average capacity. Therefore, for another stage of optimization, we try to derive an optimal speed v^* for the whole vehicle platoon where each vehicle drives with the respective $h^*(v)$.

$$\max_v \mathbb{E}s(v,h^*(v))$$

$$\min_v S(v,h^*(v)) = \tau + h^*(v) + \frac{2N(54v+1800)(h^*(v)+\tau)}{(N+1)\tau}\int_{-\inf}^{L-(h^*(v)+\tau)v}\frac{1}{\sqrt{2\pi}\sigma_x}exp(-\frac{d^2}{2\sigma_x^2})\mathbf{d}d \tag{34}$$

We try to prove its monotonicity so that the optimal value of v would be as large as limited by restrictions (if any). For any speed v_1 larger than v_0, we give a $h(v_1)$ such that:

$$(h^*(v_0)+\tau)v_0 = (h(v_1)+\tau)v_1 \tag{35}$$

$$\implies h(v_1) < h^*(v_0), \forall v_1 > v_0 \tag{36}$$

$$\begin{aligned}
S(v_1,h(v_1)) &= \tau + h(v_1) + \frac{2N(54v_1+1800)(h(v_1)+\tau)}{(N+1)\tau}\int_{-\inf}^{L-(h(v_1)+\tau)v_1}\frac{1}{\sqrt{2\pi}\sigma_x}exp(-\frac{d^2}{2\sigma_x^2})\mathbf{d}d \\
&= \tau + h(v_1) + \frac{2N(54v_0+1800\frac{v_0}{v_1})(h^*(v_0)+\tau)}{(N+1)\tau}\int_{-\inf}^{L-(h^*(v_0)+\tau)v_0}\frac{1}{\sqrt{2\pi}\sigma_x}exp(-\frac{d^2}{2\sigma_x^2})\mathbf{d}d \\
&< \tau + h^*(v_0) + \frac{2N(54v_0+1800)(h^*(v_0)+\tau)}{(N+1)\tau}\int_{-\inf}^{L-(h^*(v_0)+\tau)v_0}\frac{1}{\sqrt{2\pi}\sigma_x}exp(-\frac{d^2}{2\sigma_x^2})\mathbf{d}d \\
&= S(v_0,h^*(v_0))
\end{aligned} \tag{37}$$

$$\implies S(v_1,h^*(v_1)) \le S(v_1,h(v_1)) < S(v_0,h^*(v_0)) \tag{38}$$

As shown in (38), the average capacity grows up with the speed that the vehicle platoon drives at. Therefore, in terms of traffic efficiency and benefits, as long as the mechanical performance and control ability of vehicles satisfy, the platoon should drive at the highest available speed.

The result of this second stage optimization could be seen in Figure 8

In addition, the restrictions on speed may also come from road conditions, such as the curvature, slope, unevenness, etc. Driving at a higher speed on an unmatched road will not only affect the comfort, but also seriously affect the safety, and then reduce the road capacity at the same time. The matching of people, roads and vehicles would be one of the problems worth discussing in the future research of intelligent transportation systems.

CONCLUSION

In this paper, we evaluated the influence of microscopic robotic errors of autonomous vehicles on the macroscopic traffic safety and efficiency performance. The systematic errors embedded in AV operations, especially in the perception module contributes to their stochastic deviation from the designed movement trajectory. The random movements then become of a source of collisions, which contributes to the accident-inclusive capacity of autonomous traffic.

The model framework is then demonstrated in the car-following scenario, in which Newell's model was used to describe AVs' car following behaviors with observation errors, which is assumed to follow Gaussian distribution. It then allows us to derive the probability of rear-end collisions originated from uncertainties in following distances. By incorporating other factors such as roadway conditions and collision clearance time, the expectation of accident-inclusive traffic capacity is established mathematically, as a function of speed and time headway. Further discus-

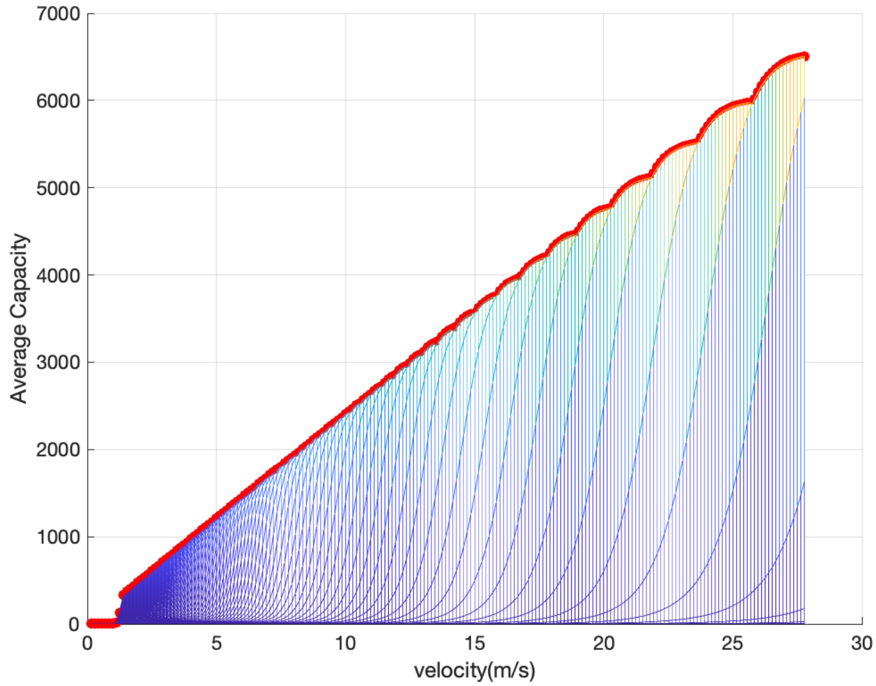

FIGURE 8 This figure shows the result of this second stage optimization. Each line shows capacity with same headway. Red scatters indicate the optimal capacities at each speed. Together, they show a monotonic increase.

sion were presented, regarding the influence from number of lanes, length of vehicle, precision of sensors and processing time step. Moreover, we formulated a two-stage optimization problem to determine the optimal safe time headway for a single AV and the optimal speed of the whole platoon, intending to maximize the expected capacity. The analysis shows that the accident-inclusive traffic capacity is monotone to vehicle speed, while the global optimum value of safe time headway could be implicitly formulated, and numerically represented, given every possible speed choice.

Our future work will continue the substantiation of the car-following scenario under robotic uncertainty, where more realistic high-order car-following models will be adopted to further refine the propagation of robotic error from perception to the motion, under which the resulted stochastic acceleration and velocity can be defined. Additionally, we plan to design and conduct experiments to reveal the distribution and nature of the perceptual errors in practice, which in turn validate conclusions of the model. The richness of the proposed model framework also provides a possibility to investigates optimal strategies other than maximizing the average capacity, the analysis, safe driving strategies that guarantee traffic efficiency, economic benefits, managerial insights on AV regulations, will also be performed in our future studies.

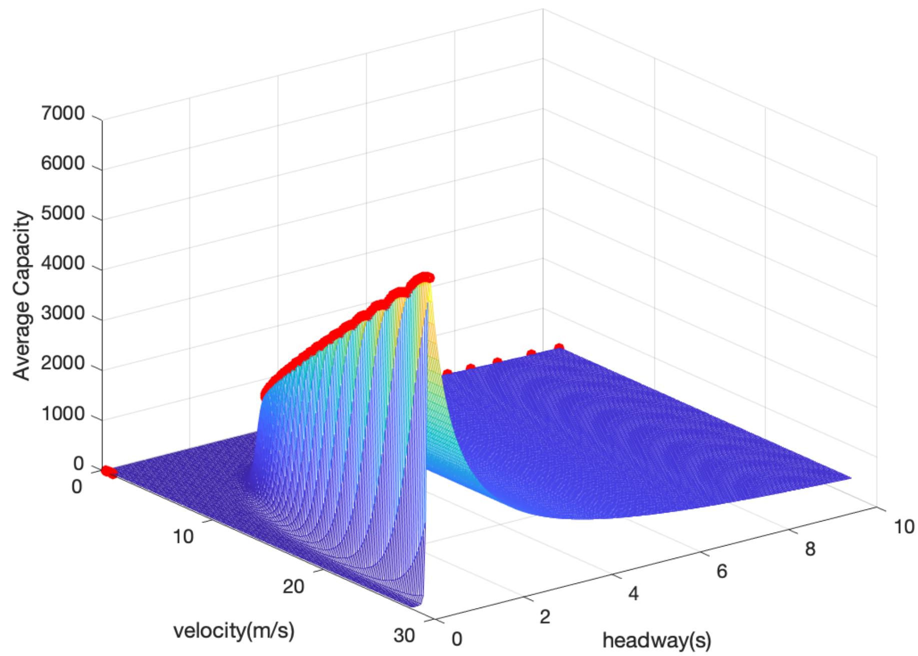

FIGURE 9 This figure shows the general view of this two stage optimization to enlarge the capacity with the growth of speed and corresponding decrease of headway.

REFERENCES

1. Fernandes, P. and U. Nunes, Platooning with IVC-enabled autonomous vehicles: Strategies to mitigate communication delays, improve safety and traffic flow. *IEEE Transactions on Intelligent Transportation Systems*, Vol. 13, No. 1, 2012, pp. 91–106.
2. Jiménez, F., J. E. Naranjo, J. J. Anaya, F. García, A. Ponz, and J. M. Armingol, Advanced driver assistance system for road environments to improve safety and efficiency. *Transportation research procedia*, Vol. 14, 2016, pp. 2245–2254.
3. Mueller, A. S., J. B. Cicchino, and D. S. Zuby, What humanlike errors do autonomous vehicles need to avoid to maximize safety? *Journal of safety research*, Vol. 75, 2020, pp. 310–318.
4. Morando, M. M., Q. Tian, L. T. Truong, and H. L. Vu, Studying the safety impact of autonomous vehicles using simulation-based surrogate safety measures. *Journal of advanced transportation*, Vol. 2018, 2018.
5. Van Arem, B., C. J. Van Driel, and R. Visser, The impact of cooperative adaptive cruise control on traffic-flow characteristics. *IEEE Transactions on intelligent transportation systems*, Vol. 7, No. 4, 2006, pp. 429–436.
6. Talebpour, A. and H. S. Mahmassani, *Influence of autonomous and connected vehicles on stability of traffic flow*, 2015.
7. Chen, D., S. Ahn, M. Chitturi, and D. A. Noyce, Towards vehicle automation: Roadway capacity formulation for traffic mixed with regular and automated vehicles. *Transportation research part B: methodological*, Vol. 100, 2017, pp. 196–221.

8. Seo, T. and Y. Asakura, Endogenous market penetration dynamics of automated and connected vehicles: Transport-oriented model and its paradox. *Transportation Research Procedia*, Vol. 27, 2017, pp. 238–245.
9. Metz, D., Developing policy for urban autonomous vehicles: Impact on congestion. *Urban Science*, Vol. 2, No. 2, 2018, p. 33.
10. Levinson, J., J. Askeland, J. Becker, J. Dolson, D. Held, S. Kammel, J. Z. Kolter, D. Langer, O. Pink, V. Pratt, et al., Towards fully autonomous driving: Systems and algorithms. In *2011 IEEE intelligent vehicles symposium (IV)*, IEEE, 2011, pp. 163–168.
11. Jo, K., J. Kim, D. Kim, C. Jang, and M. Sunwoo, Development of autonomous car—Part I: Distributed system architecture and development process. *IEEE Transactions on Industrial Electronics*, Vol. 61, No. 12, 2014, pp. 7131–7140.
12. Jo, K., J. Kim, D. Kim, C. Jang, and M. Sunwoo, Development of autonomous car—Part II: A case study on the implementation of an autonomous driving system based on distributed architecture. *IEEE Transactions on Industrial Electronics*, Vol. 62, No. 8, 2015, pp. 5119–5132.
13. Thrun, S., Bayesian landmark learning for mobile robot localization. *Machine learning*, Vol. 33, No. 1, 1998, pp. 41–76.
14. Roumeliotis, S. I. and G. A. Bekey, Bayesian estimation and Kalman filtering: A unified framework for mobile robot localization. In *Proceedings 2000 ICRA. Millennium Conference. IEEE International Conference on Robotics and Automation. Symposia Proceedings (Cat. No. 00CH37065)*, IEEE, 2000, Vol. 3, pp. 2985–2992.
15. Zhou, Y., S. Ahn, M. Chitturi, and D. A. Noyce, Rolling horizon stochastic optimal control strategy for ACC and CACC under uncertainty. *Transportation Research Part C: Emerging Technologies*, Vol. 83, 2017, pp. 61–76.
16. Van Brummelen, J., M. O'Brien, D. Gruyer, and H. Najjaran, Autonomous vehicle perception: The technology of today and tomorrow. *Transportation research part C: emerging technologies*, Vol. 89, 2018, pp. 384–406.
17. Kocić, J., N. Jovičić, and V. Drndarević, Sensors and sensor fusion in autonomous vehicles. In *2018 26th Telecommunications Forum (TELFOR)*, IEEE, 2018, pp. 420–425.
18. Pendleton, S. D., H. Andersen, X. Du, X. Shen, M. Meghjani, Y. H. Eng, D. Rus, and M. H. Ang Jr, Perception, planning, control, and coordination for autonomous vehicles. *Machines*, Vol. 5, No. 1, 2017, p. 6.
19. Shladover, S. E. and C. Nowakowski, Regulatory challenges for road vehicle automation: Lessons from the california experience. *Transportation research part A: policy and practice*, Vol. 122, 2019, pp. 125–133.
20. Kyriakidis, M., R. Happee, and J. C. de Winter, Public opinion on automated driving: Results of an international questionnaire among 5000 respondents. *Transportation research part F: traffic psychology and behaviour*, Vol. 32, 2015, pp. 127–140.
21. Howard, D. and D. Dai, Public perceptions of self-driving cars: The case of Berkeley, California. In *Transportation research board 93rd annual meeting*, 2014, Vol. 14, pp. 1–16.
22. Penmetsa, P., P. Sheinidashtegol, A. Musaev, E. K. Adanu, and M. Hudnall, Effects of the autonomous vehicle crashes on public perception of the technology. *IATSS research*, Vol. 45, No. 4, 2021, pp. 485–492.

23. Liu, J. and J.-M. Park, “Seeing is Not Always Believing”: Detecting Perception Error Attacks Against Autonomous Vehicles. *IEEE Transactions on Dependable and Secure Computing*, Vol. 18, No. 5, 2021, pp. 2209–2223.
24. Wang, J., L. Zhang, Y. Huang, and J. Zhao, Safety of autonomous vehicles. *Journal of advanced transportation*, Vol. 2020, 2020.
25. Krauß, S., Microscopic modeling of traffic flow: Investigation of collision free vehicle dynamics, 1998.
26. Jabari, S. E. and H. X. Liu, A stochastic model of traffic flow: Theoretical foundations. *Transportation Research Part B: Methodological*, Vol. 46, No. 1, 2012, pp. 156–174.
27. Xu, T. and J. Laval, Statistical inference for two-regime stochastic car-following models. *Transportation Research Part B: Methodological*, Vol. 134, 2020, pp. 210–228.
28. Qu, X., J. Zhang, and S. Wang, On the stochastic fundamental diagram for freeway traffic: model development, analytical properties, validation, and extensive applications. *Transportation research part B: methodological*, Vol. 104, 2017, pp. 256–271.
29. Daganzo, C. F. and N. Geroliminis, An analytical approximation for the macroscopic fundamental diagram of urban traffic. *Transportation Research Part B: Methodological*, Vol. 42, No. 9, 2008, pp. 771–781.
30. Newell, G. F., A simplified car-following theory: a lower order model. *Transportation Research Part B: Methodological*, Vol. 36, No. 3, 2002, pp. 195–205.
31. Dougald, L. E., R. Venkatanarayana, N. J. Goodall, et al., *Traffic incident management quick clearance guidance and implications*. Virginia Transportation Research Council, 2016.
32. Smith, K. and B. L. Smith, Forecasting the clearance time of freeway accidents, 2002.